ARTICLES

Journal of Semiconductors
(2021) 42, 052701
doi: 10.1088/1674-4926/42/5/052701

WO_3 passivation layer-coated nanostructured TiO_2: An efficient defect engineered photoelectrode for dye sensitized solar cell

Arya Babu, Arya Vasanth, Shantikumar Nair, and Mariyappan Shanmugam†

Amrita Centre for Nanosciences and Molecular Medicine, Amrita Vishwa Vidyapeetham, Kochi, Kerala - 682041, India

Abstract: Major loss factors for photo-generated electrons due to the presence of surface defects in titanium dioxide (TiO_2) were controlled by RF-sputtered tungsten trioxide (WO_3) passivation. X-ray photoelectron spectroscopy assured the coating of WO_3 on the TiO_2 nanoparticle layer by showing Ti 2p, W 4f and O 1s characteristic peaks and were further confirmed by X-ray diffraction studies. The coating of WO_3 on the TiO_2 nanoparticle layer did not affect dye adsorption significantly. Dye sensitized solar cells (DSSCs) fabricated using WO_3-coated TiO_2 showed an enhancement of ~10% compared to DSSCs fabricated using pristine TiO_2-based photo-electrodes. It is attributed to the WO_3 passivation on TiO_2 that creates an energy barrier which favored photo-electron injection by tunneling but blocked reverse electron recombination pathways towards holes available in highest occupied molecular orbital of the dye molecules. It was further evidenced that there is an optimum thickness (duration of coating) of WO_3 to improve the DSSC performance and longer duration of WO_3 suppressed photo-electron injection from dye to TiO_2 as inferred from the detrimental effect in short circuit current density values. RF-sputtering yields pinhole-free, highly uniform and conformal coating of WO_3 onto any area of interest, which can be considered for an effective surface passivation for nanostructured photovoltaic devices.

Key words: charge transport; recombination; tungsten oxide; solar cell; interface; defects

Citation: A Babu, A Vasanth, S Nair, and M Shanmugam, WO_3 passivation layer-coated nanostructured TiO_2: An efficient defect engineered photoelectrode for dye sensitized solar cell[J]. *J. Semicond.*, 2021, 42(5), 052701. http://doi.org/10.1088/1674-4926/42/5/052701

1. Introduction

The most important technological arrival of nanotechnology has endorsed multifarious nanostructured functional materials for energy conversion applications[1–4]. Nanostructured functional materials have been showing superior characteristics in terms of structural, optical, electrical and mechanical perspectives[5–8]. Size-dependent properties of nanomaterials and their consequences on various applications have been realized as a potential possible approach to improve performance of resulting products including photovoltaics, sensors, batteries and light-emitting diodes[2, 9–11]. However, it has been observed that nanostructures, such as particles, fibers and planar materials, exhibit surface sensitive characteristics due to the presence of chemically unsaturated defect states which are established through the modified surface-to-volume ratio[12–16]. Such remarkable changes over the surface of functional materials lead to unavoidable degeneracies, including surface states which can have energy distribution throughout the bandgap of resulting materials[17–21]. Surface states in a material plays a critical role on charge transport and recombination as they are electronically active mostly in the vicinity of band-edges[22, 23]. However, nanostructured functional materials cannot be avoided in energy conversion devices as they show dominant optical and electrical transport characteristics which are highly preferred specifically for light-matter interaction[24–26]. Thus, alternate measures are required to employ such attractive materials for energy-related applications and those measures are expected to control the detrimental effects of surface defects on charge transport to minimize the recombination loss. A surface with active unsaturated dangling bonds is highly sensitive to charge transport in solar cells and thus it is an essential factor to passivate/modify using appropriate methods[27–30].

A variety of metal oxides and dielectrics were used in DSSCs to control the recombination at TiO_2/dye/electrolyte interfaces[30–38]. Thickness, dielectric properties, surface coverage and electronic quality of the passivation layers have been studied and reported to be considered as dominant factors which determine the ability to control the defects[39–44]. Wet-chemical methods such as hydrothermal process, physical vapor deposition techniques, including RF/DC sputtering, electron beam/thermal evaporation and chemical vapor deposition, were widely used to apply passivation on functional materials such as TiO_2 in DSSCs[45–49]. Atomic layer deposition has been identified as a superior technique to passivate nanostructured defective material as it often yields ultra-thin (few atomic layers) high-quality dielectrics which can be conformally coated onto any randomly distributed nanostructures[50, 51]. The highly conformal surface coverage results in efficient passivation which controls the detrimental role of defects on charge transport in DSSCs[52–54].

The present work identified tungsten oxide (WO_3) as a possible wide bandgap material which can be used for effective surface passivation on TiO_2 to modify the surface to achieve better control over defects. Results showed the possibility of improving DSSC performance by coating WO_3 via RF-sputter-

Correspondence to: M Shanmugam, mshanmugham@aims.amrita.edu
Received 20 AUGUST 2020; Revised 1 DECEMBER 2020.

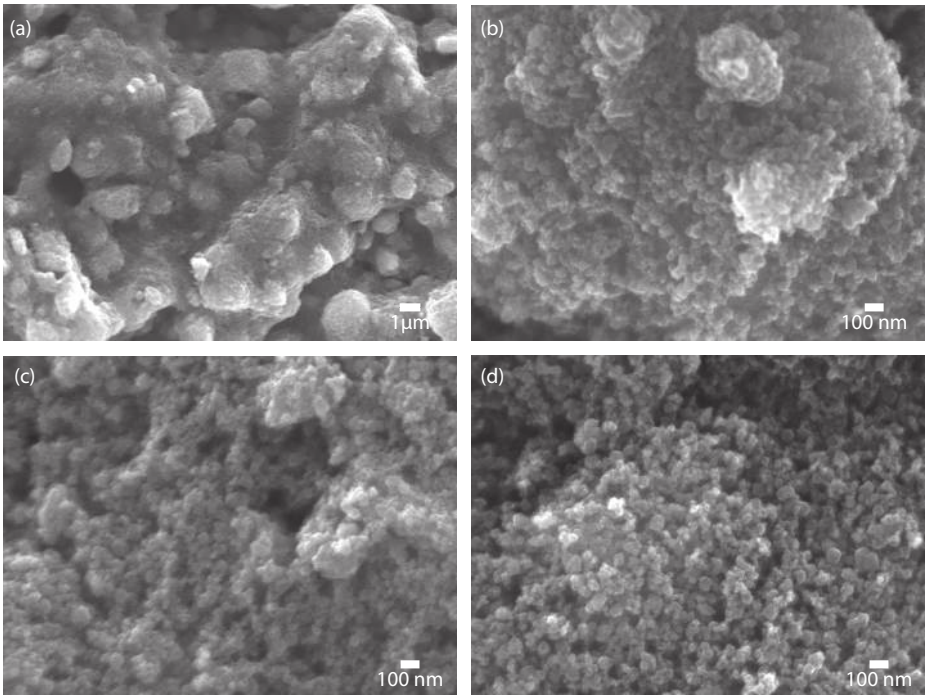

Fig. 1. Surface morphology of pristine TiO_2 at the magnifications of (a) 1000× and (b) 40 000× showing macroscopic clusters and agglomerated particles respectively, (c, d) WO_3 coated TiO_2 nanoparticles layer showing randomly distributed TiO_2 nanoparticles and the porous nature.

ing on TiO_2 in which defects are most dominating in terms of interfacial recombination.

2. Experimental section

Commercially available fluorine-doped tin oxide (FTO) glass substrates were used for DSSC fabrication process. The FTO-coated glass substrates were cleaned by sonicating them in soap solution for 15 min, then in DI water and finally with ethanol for 15 min to remove all sort of contaminations. The cleaned FTO-coated glass substrates were kept in an oven for drying at 72 ˚C. Colloidal TiO_2 paste was prepared by mixing the required amount of TiO_2 powder (Sigma Aldrich, 99.9% purity) and polyethylene glycolate (PEG). Both were mixed and ground thoroughly using a mortar and pestle until a required form of colloidal paste was obtained. TiO_2 colloidal paste was doctor-bladed onto FTO-coated glass substrates using adhesive tape as a shadow-mask, which were removed after making the TiO_2 films. Colloidal TiO_2 films coating the FTO samples were then annealed at 450 ˚C for 3 h with a ramp rate of 3 ˚C per minute.

WO_3 thin film was coated on TiO_2 nanoparticle films using the RF sputtering technique. Samples were fixed on the substrate holder using temperature-sustainable, vacuum-compatible Kapton tape. They were placed in the RF-sputter chamber in which tungsten was used as target with oxygen as a bombarding process gas. The oxygen gas flow rate was maintained at 70 sccm with a FR-power of 25 W. To assess the effect of thickness of WO_3 surface passivation on TiO_2, the present study varied the thickness values of WO_3 to 15, 22, and 30 nm on TiO_2. This thickness variation was achieved by varying the duration of WO_3 coating on TiO_2 for 7, 10, and 15 min. The WO_3-coated TiO_2 nanoparticle layer on FTO was removed from the RF-sputter chamber and annealed at 120 ˚C.

In the present work, two categories of DSSCs were fabricated using (i) pristine TiO_2 and (ii) WO_3-coated TiO_2 to validate the effect of WO_3 passivation on TiO_2 nanoparticle layer in DSSC performance. Ruthenium-based N719 dye was prepared using a mixture of 50 mL of tert-butyl alcohol and 50 mL of acetonitrile. Then, 0.5 mM of N719 dye (59.43 mg for 100 mL) was added and stirred for 30 min to make the required homogeneous N719 dye. The pristine TiO_2 and WO_3-coated TiO_2 samples prepared on FTO-coated glass substrates were immersed in dye solution to sensitize. DSSCs were fabricated using N719-adsorbed pristine TiO_2 and WO_3-coated TiO_2 as photo-anodes to compare the effect of WO_3 passivation. Hole-transporting iodide/tri-iodide was used as an electrolyte along with a platinum counter electrode for the DSSCs. The only difference between the two categories of DSSCs was the WO_3 passivation on the TiO_2 nanoparticle layer.

Surface morphology of the pristine and WO_3-coated TiO_2 samples were characterized using a JSN 7610S Plus JEOL-JSM-6490-LA scanning electron microscope (FESEM). X-ray photoelectron spectroscopy (XPS) used a Kratos Analytical unit. X-ray diffraction (XRD) patterns of the WO_3 coated samples were obtained using PANalytical X'Pert PRO X-Ray Diffractometer. UV–visible optical spectra of the samples were obtained in a Perkin Elmer Lambda-750 UV–visible spectrometer. The fabricated DSSCs were characterized under 1-Sun illumination (AM 1.5 G) in a Newport Oriel Class A solar simulator to measure required *J–V* characteristics using a Keithley-2420 digital source meter.

3. Results and discussion

Figs. 1(a) and 1(b) show surface morphology of the TiO_2 nanoparticle layer coated on the FTO substrate for DSSC fabrication. Macroscopic clustered TiO_2 was observed at the low (1000×) magnification in Fig. 1(a), and a further magnified im-

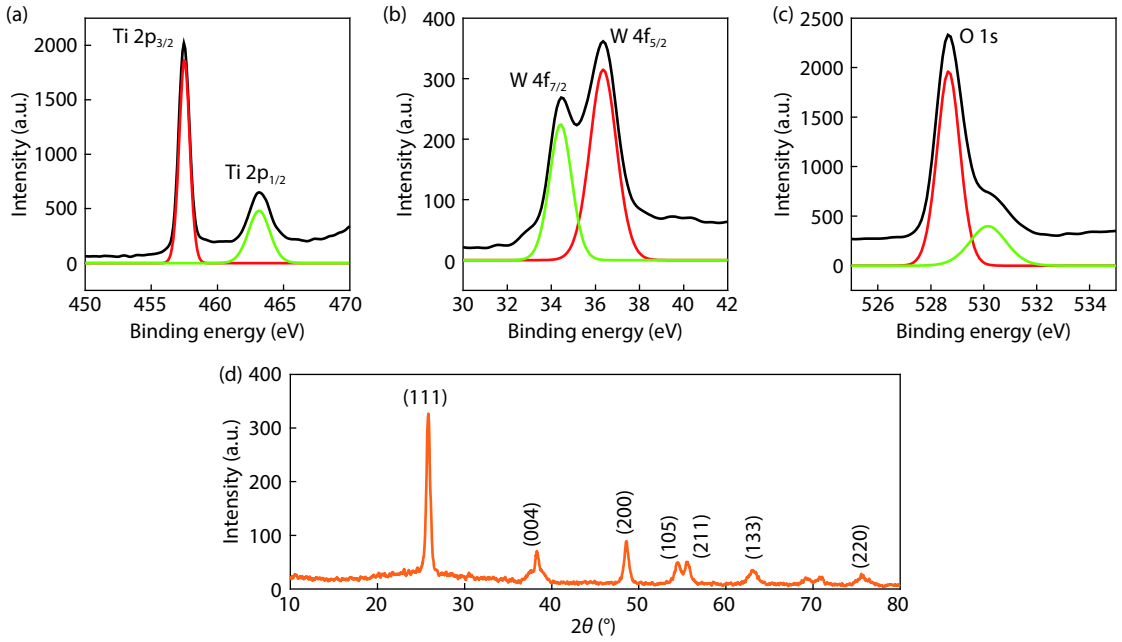

Fig. 2. (Color online) (a–c) High resolution XPS scans showing Ti 2p, W 4f and O 1s peaks from the WO_3 coated TiO_2 sample. (d) XRD pattern obtained from the same sample.

age exhibited smaller size TiO_2 particles agglomerated on the macroscopic clusters as shown in Fig. 1(b) which was obtained at the magnification of 40 000×. While the lower magnified image exhibited a macroscopic cluster film, the higher one showed the nanoparticles agglomerated as clusters. Figs. 1(c) and 1(d) were obtained from the TiO_2 nanoparticle layer after coating the WO_3 passivation layer at 15 and 30 nm, respectively. It is evident that the coating of thin WO_3 on the TiO_2 nanoparticle layer did not change the morphology significantly in terms of surface morphology. The WO_3 coating was performed by RF-sputtering, which is a gas-phase plasma assisted physical vapor deposition process to achieve uniform coating of functional material. The surface morphology images shown in Figs. 1(c) and 1(d) clearly addressed the pristine nature of the TiO_2 nanoparticle layer was not modified as the RF-sputtering process uniformly covered the TiO_2 nanoparticles and the coating did not block the porosity of the TiO_2, as can be seen in Figs. 1(a) and 1(b). In general, the surface passivation coating is applied on nanostructured functional materials in which defects are playing a dominated role on charge transport characteristics and deteriorates the performance of the resulting solar cells. Thus, it is essential to coat the surface passivation layer but if it is too thick or not uniform then the surface passivation layer itself might block the charge transport and thus recombination would dominate. In the present study, the surface morphology images prove that WO_3 did not affect TiO_2 morphology as it was thin enough and uniform.

Fig. 2 shows results from XPS and XRD studies performed on the WO_3-coated TiO_2 nanoparticle layer. Fig. 2(a) shows a high-resolution XPS scan obtained from the sample showing Ti 2p peaks. Specifically, Ti $2p_{3/2}$ and Ti $2p_{1/2}$ were 457.4 and 463.1 eV respectively, showing the spin-orbital splitting of photoelectrons. The binding energy difference between two peaks was 5.7 eV. Fig. 2(b) shows a high-resolution XPS scan of tungsten (W) which belongs to the WO_3 passivation layer on the TiO_2 nanoparticle layer. The spin-orbital splitting of photoelectrons exhibited W $4f_{7/2}$ and W $4f_{5/2}$ at the binding energy values of 34.4 and 36.3 eV respectively. The energy difference between the two peaks was observed to be 1.9 eV. The high-resolution XPS scan showing O 1s spectrum obtained from the sample is shown in Fig. 2(c). The peak occurred at 528.7 eV. All these characteristic peaks, identified with respect to their binding energy values, confirmed the WO_3 coating on the TiO_2 nanoparticle layer. Fig. 2(d) shows XRD pattern of the WO_3-coated TiO_2 nanoparticle layer. The XRD peak appeared at 2θ of 25.8° represents (101) which corresponds to the anatase TiO_2 phase and this was confirmed from JCPDS-84-1286. The TiO_2 is considered to be phase pure as it did not show the rutile phase at 2θ value of 27.36°. Further the XRD peaks at 2θ values of 38.3° (004), 48.5° (200) and 55.6° (211) also assert the TiO_2 nanoparticle layer. The indices (105), (133) and (220) at 2θ values of 54.4°, 63.1°, 75.5° represent the WO_3 thin film coating on the TiO_2 nanoparticle layer. Thus, the XRD pattern obtained from the WO_3 passivation thin film-coated TiO_2 nanoparticle layer also confirmed both the functional materials with respective to their characteristic peaks.

Fig. 3(a) shows photographs of the pristine TiO_2 nanoparticle layer along with 15, 22, 30 nm WO_3-coated TiO_2. It was very obvious that WO_3 passivation was thin enough, which did not change the TiO_2 much in terms of the color. However, it was very clear from the picture that WO_3 was coated on the surface of the TiO_2 nanoparticle film. In this study, WO_3 was coated on TiO_2 to modify/suppress the defects which are actively participating in the charge transport process in DSSCs. Thus, it was a genuine expectation that WO_3 should not affect the dye adsorption on the surface of TiO_2. The photograph shown in Fig. 3(b) shows the pristine TiO_2 nanoparticle layer along with 15, 22, and 30 nm WO_3-coated TiO_2 after the dye loading process. It provided evidence that coating of WO_3 on the TiO_2 nanoparticle layer did

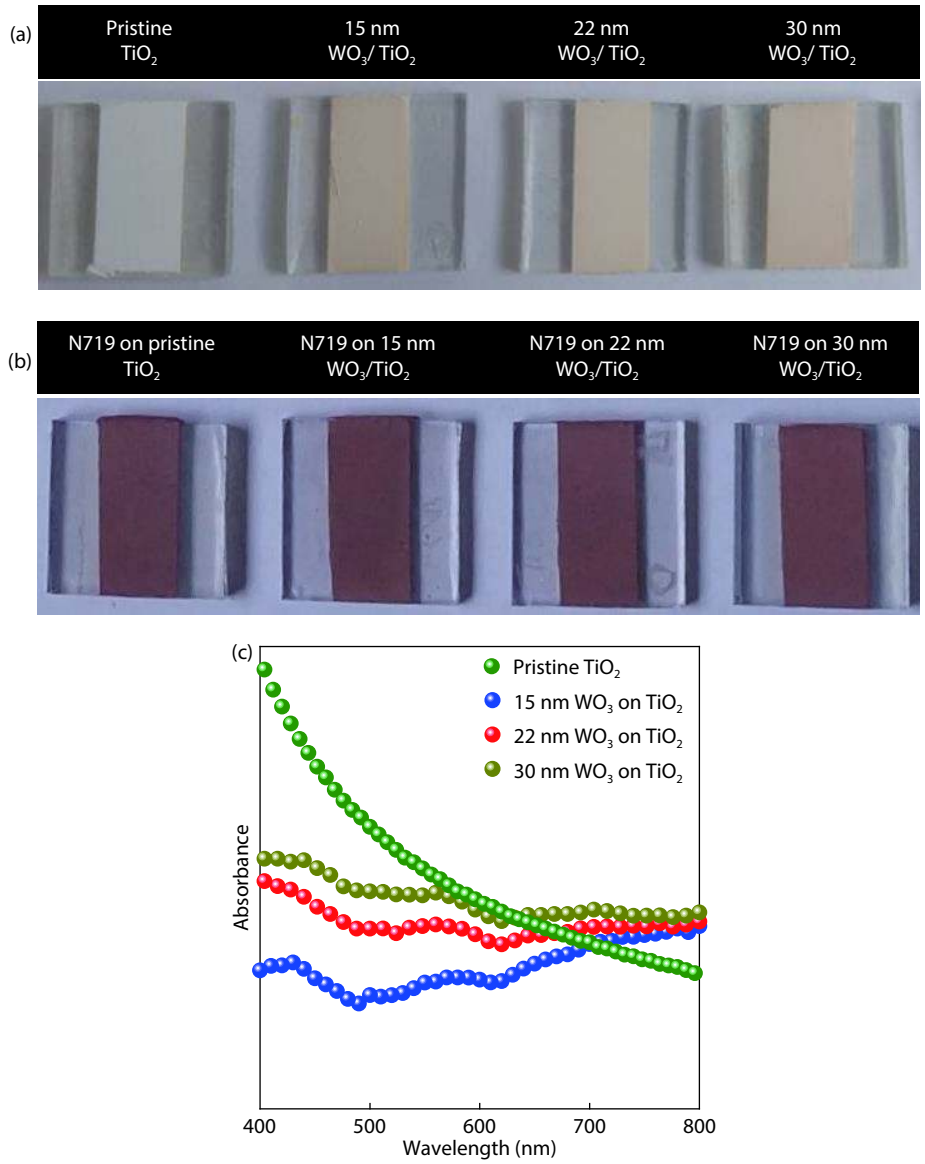

Fig. 3. (Color online) Digital photographic images of (a) TiO_2 nanoparticle layer coated on FTO covered glass substrates showing the deposition of WO_3 surface passivation layer with different thickness values. (b) Photographs of the samples after N719 dye coating confirming the WO_3 did not affect the loading much. (c) UV–visible absorption spectra of the samples.

not affect the dye loading significantly. In general, a surface passivation layer is expected to control the defects in semiconductors to improve the charge transport characteristics to yield high performance photovoltaic devices. If the dye loading into the TiO_2 nanoparticle layer is impeded by WO_3, then exciton generation will be reduced significantly which, in turn, would result in lower photo-current and overall performance. Fig. 3(c) shows UV–visible optical absorption spectroscopic measurements performed on the pristine TiO_2 nanoparticle layer in comparison with TiO_2 samples coated with the 15, 22, and 30 nm WO_3 surface passivation layer. As shown in the Fig. 3(c), the pristine and WO_3-coated TiO_2 did not show any significant absorption in the spectral window of 400–800 nm in which a major portion of visible energy photons are available. Thus, passivating TiO_2 by WO_3 will not impede visible spectral photons to reach dye molecules to generate excitons. Thus, WO_3 coating on TiO_2 can be categorized as an advantage for DSSC operation in terms of defect passivation but has no disadvantage in terms of absorption loss due to the optimum band structure characteristics. In DSSCs, incident photons enter through a transparent electrode, FTO, and travel through the TiO_2 nanoparticle layer to reach organic dye to generate excitons. Passivation layers are coated on TiO_2 in DSSCs to control defects. If the passivation layer scatters or disperses photons between TiO_2 and dye, it will lead to major optical loss which would affect the photocurrent generation. Thus, it is important to confirm the passivation layer does not interact with incident photons in the visible spectral range. Further, UV–visible spectra of WO_3-coated TiO_2 samples exhibited that absorption at the high energy spectral region was significantly suppressed after WO_3 coating. WO_3 exhibits an optical bandgap in the range of 2.6–3 eV. When pristine TiO_2 showed absorption in the high energy range, WO_3 coating suppressed the exciton generation at this specific range due to the heterostructure alignment in the band-structure[55]. It could be attributed to the thermalization effect which also contributed to the increment in the absorption of photons in the longer wavelength regions. This ef-

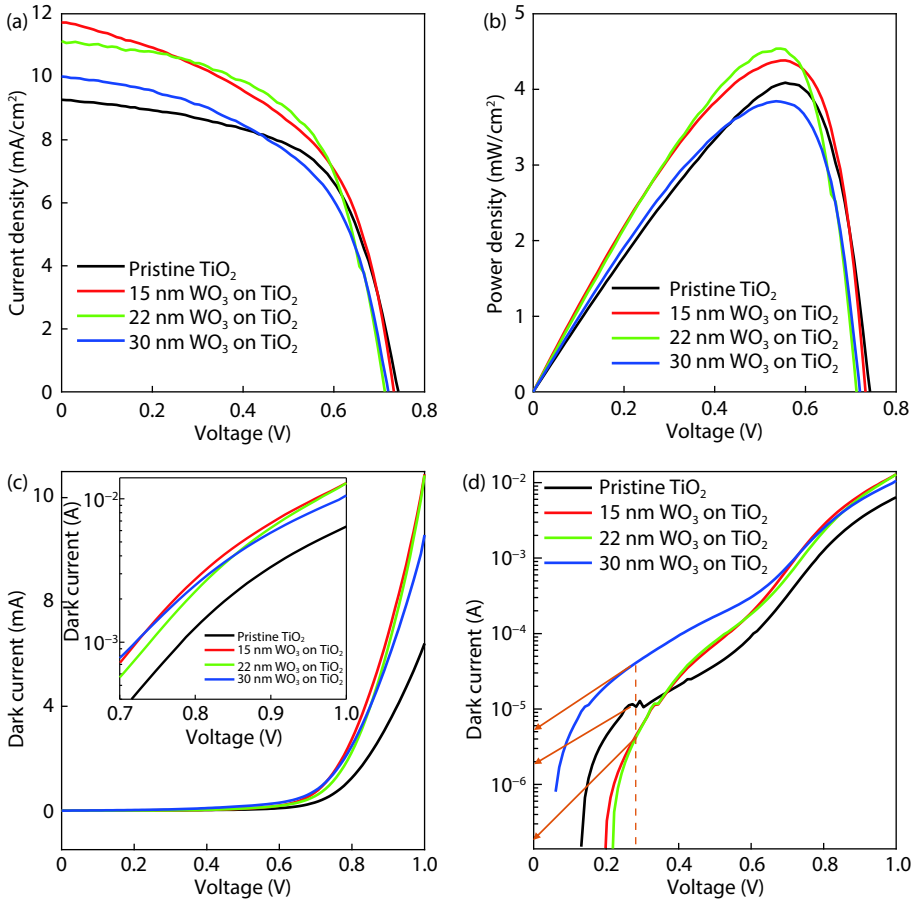

Fig. 4. (Color online) (a) *J–V* characteristics of the DSSC with and without WO_3 passivation on TiO_2. (b) Comparison of P_{MAX} of DSSCs, dark current characteristics of DSSCs in (c) linear and (d)semi-log scale showing the saturation current values.

Table 1. Photovoltaic parameters of the DSSCs measured under AM1.5 illumination level.

DSSCs	WO_3 coating duration (min)	V_{OC} (mV)	J_{SC} (mA/cm^2)	FF (%)	η (%)	SD in η
Pristine TiO_2		745	09.3	59.0	4.1	0.05
15 nm WO_3 on TiO_2	7	732	11.8	50.8	4.3	0.06
22 nm WO_3 on TiO_2	10	712	11.1	57.2	4.5	0.10
30 nm WO_3 on TiO_2	15	720	10.0	53.1	3.8	0.09

fect was observed in all three TiO_2 samples with WO_3 coating.

Fig. 4(a) shows illuminated *J–V* characteristics of the DSSCs which used pristine TiO_2 as a photo-anode along with the WO_3 passivation layer-coated TiO_2. The illuminated *J–V* characteristics of the DSSCs showed that coating of WO_3 on the TiO_2 nanoparticle played a significant role in terms of all photovoltaic parameters including open circuit voltage (V_{OC}), short circuit current density (J_{SC}), fill factor (*FF*) and efficiency (η). All the key photovoltaic parameters measured under AM 1.5 illumination are listed in Table 1 along with standard deviation in η. The reference DSSC, which used a pristine TiO_2-based photo-anode (no WO_3 coating), resulted in V_{OC}, J_{SC}, *FF* and η of 745 mV, 9.3 mA/cm^2, 59.0%, and 4.1% respectively. The DSSC, which used 22 nm coating of WO_3 on TiO_2 as a photo-anode, resulted in V_{OC}, J_{SC}, *FF* and η of 712 mV, 11.1 mA/cm^2, 57.2%, and 4.5%, respectively. This is approximately 10% enhancement in η due to the increment in J_{SC}. As can be seen in Table 1, further increment in the duration of WO_3 coating on TiO_2 affected photovoltaic parameters significantly. It can be directly attributed to the reduction in J_{SC} by creating a thicker energy barrier between the TiO_2 and dye where the charge carrier injection occurred. It is well known that if the energy barrier thickness increases, then tunneling probability would decrease. Thus, an optimum thickness of the passivation layer is required to passivate the defects. In the present study, it was found that 10 min WO_3 coating on TiO_2 performed better than other DSSCs.

Fig. 4(b) shows power density–voltage characteristics of the reference DSSCs along with DSSCs used WO_3 passivation showing the maximum power point (P_{MAX}) values. It was noticed that DSSC used 10 min of WO_3 passivation on TiO_2 resulted in 4.5 mW/cm^2 while the reference DSSC exhibited 4 mW/cm^2. This is one of the parameters along with the increment in J_{SC} improved the ~10% enhancement in η for the DSSC with 22 nm WO_3 passivation on TiO_2. The DSSC with 15 min of WO_3 passivation showed 3.8 mW/cm^2. It clearly indicated that increasing thickness of WO_3 affected the P_{MAX} and thus the detrimental effect on photovoltaic performance. Fig. 4(c) shows dark current–voltage characteristics of the DSSCs with a semi-log plot of the same in the higher applied range of 0.7 to 1 V. It is possible to assess the electronic quality of interfaces in DSSCs through dark saturation current (I_O)

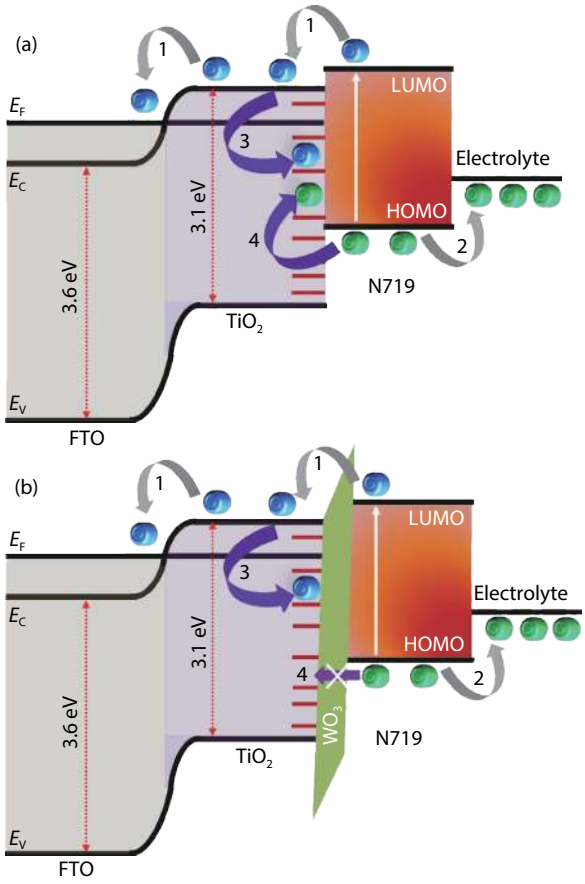

Fig. 5. (Color online) Schematic illustration of (a) FTO/TiO_2/dye/electrolyte and (b) FTO/TiO_2/WO_3/Dye/electrolyte interfaces in DSSCs showing electron–hole transport and recombination mediated by defects in TiO_2.

which can be obtained from the general $I_D = I_O\exp(qV/kT–1)$, where I_D and I_O are current density and saturation current respectively under dark conditions. The parameters in equation q, V, k and T are electronic charge, applied bias to the DSSCs, Boltzmann constant and temperature at which the DSSCs work respectively. It is well known that DSSCs with good quality interfaces exhibit higher I_O values at higher applied bias regions, lower I_O values at lower and medium forward bias regions. Increasing I_O in the low and medium forward bias regions can directly be attributed to the defect dominated charge transport. Thus, the parameter (I_O) needs to be suppressed to obtain a DSSC with improved photovoltaic performance. Inset in Fig. 4(c) clearly showed the DSSC with 10 min WO_3 coating resulted in higher I_O value compared with other DSSCs. Fig. 4(d) shows semi-log plots of dark current characteristics of the reference DSSC along with DSSC used WO_3 passivation. We have chosen the applied bias region close to 0.3 V to consider the I_O values for the DSSCs. It is evident that DSSC with 10 min of WO_3 passivation on TiO_2 exhibited 1×10^{-7} A, which is 20 times lower than the I_O values showed by reference DSSC which was 2×10^{-6} A. In this calculation, 0.3 V applied bias has been considered to extract the I_O values for all DSSCs for the reason that a linear dark current increment was observed in the semi-log plot as shown in Fig. 4(d). If the dark current is highly linear in the log-scale, it is a perfect exponential diode characteristic feature. Thus, the applied bias of 0.3 V has been used to extract I_O values.

Figs. 5(a) and 5(b) show the energy level diagram representing FTO/TiO_2/dye/electrolyte and FTO/TiO_2/WO_3/Dye/electrolyte interfaces respectively. The only difference between the two categories of DSSCs examined in the present work was WO_3 passivation on TiO_2. Thus, the variation in photovoltaic performance is directly attributed to the ability of WO_3 to passivate defects in TiO_2. Photo-generated electrons in the lowest unoccupied molecular orbital (LUMO) of the dye need to be injected into the conduction band edge of TiO_2 (E_C) in which they are all transported to reach the FTO electrode by diffusion as represented by process (1). Meanwhile, the holes from the highest occupied molecular orbital (HOMO) of the dye will be regenerated by the electrolyte as shown in process (2). These two categories are electron and hole transport, which eventually contribute to photo-current in DSSCs. However, the photo-electrons in the bulk of TiO_2 nanoparticle layer can be trapped by defects present in the bandgap of TiO_2 as illustrated by process (3). If the trap states, which are close to the trapped electron, can trap a hole from the HOMO of the dye as shown in process (4), then electron-hole recombination will occur at the bandgap of TiO_2 mediated by defects. Fig. 5(b) shows the possible changes that can occur at the electron–hole transport and recombination kinetics after coating the WO_3 surface passivation layer on TiO_2. The photo-generated electron injection from the LUMO of the dye will be injected through the WO_3 surface passivation layer by tunneling as the thickness is facilitating such a transport process. Photo-generated electrons in the TiO_2 further can be trapped by defects but the probability of hole trapping, process (4), is rather difficult as the WO_3 will not allow the trap states in TiO_2 to interact with holes at the HOMO of the dye. Thus, hole trapping will not occur at the TiO_2/dye interface after coating the passivation layer. The photo-generated electron will not be lost without having a hole in the bulk vicinity of TiO_2. The probability of recombination loss is expected to be suppressed by coating a thin WO_3 film on TiO_2. This situation will lead to improved DSSC performance.

4. Conclusion

A dominant recombination pathway at the TiO_2/dye interface was significantly suppressed by passivating the TiO_2 surface using RF-sputtered WO_3 film. RF-sputtering is a versatile technique to coat WO_3 surface passivation on the TiO_2 nanoparticle layer without blocking the porosity. DSSC with WO_3 passivation exhibited ~10% enhancement in performance. Results from DSSCs confirmed that there is an optimum thickness of WO_3, at which the electron-hole transport was facilitated while the recombination probability was reduced.

Acknowledgements

We thank the Amrita Centre for Nanosciences for providing us with the PVD cluster equipment to coat various functional thin films for the energy conversion technology development.

References

[1] Mlinar V. Engineered nanomaterials for solar energy conversion. Nanotechnology, 2013, 24, 042001

[2] Kumar S, Nehra M, Deep A, et al. Quantum-sized nanomaterials

for solar cell applications. Renew Sustain Energy Rev, 2017, 73, 821

[3] Sun H, Deng J, Qiu L B, et al. Recent progress in solar cells based on one-dimensional nanomaterials. Energy Environ Sci, 2015, 8, 1139

[4] Brennan L J, Byrne M T, Bari M, et al. Carbon nanomaterials for dye-sensitized solar cell applications: A bright future. Adv Energy Mater, 2011, 1, 472

[5] Yang N L, Zhai J, Wang D, et al. Two-dimensional graphene bridges enhanced photoinduced charge transport in dye-sensitized solar cells. ACS Nano, 2010, 4, 887

[6] Yu R, Lin Q F, Leung S F, et al. Nanomaterials and nanostructures for efficient light absorption and photovoltaics. Nano Energy, 2012, 1, 57

[7] Hu Y, Wang H, Hu B. Thinnest two-dimensional nanomaterial—graphene for solar energy. ChemSusChem, 2010, 3, 782

[8] Li W, Elzatahry A, Aldhayan D, et al. Core-shell structured titanium dioxide nanomaterials for solar energy utilization. Chem Soc Rev, 2018, 47, 8203

[9] Su S, Wu W H, Gao J M, et al. Nanomaterials-based sensors for applications in environmental monitoring. J Mater Chem, 2012, 22, 18101

[10] Sun Y M, Liu N, Cui Y. Promises and challenges of nanomaterials for lithium-based rechargeable batteries. Nat Energy, 2016, 1, 16071

[11] Gao M, Yao J C, Yan C, et al. Novel composite nanomaterials with superior thermal and pressure stability for potential LED applications. J Alloy Compd, 2018, 734, 282

[12] Ramakrishna G, Singh A K, Palit D K, et al. Dynamics of interfacial electron transfer from photoexcited quinizarin (Qz) into the conduction band of TiO_2 and surface states of ZrO_2 nanoparticles. J Phys Chem B, 2004, 108, 4775

[13] Hanzu I, Djenizian T, Knauth P. Electrical and point defect properties of TiO_2 nanotubes fabricated by electrochemical anodization. J Phys Chem C, 2011, 115, 5989

[14] Nasirpouri F, Peighambardoust N S, Samardak A, et al. Structural defect-induced bandgap narrowing in dopant-free anodic TiO_2 nanotubes. ChemElectroChem, 2017, 4, 1227

[15] Menon H, Gopakumar G, Sankaranarayanan Nair V, et al. 2D-layered MoS_2-incorporated TiO_2-nanofiber- based dye-sensitized solar cells. ChemistrySelect, 2018, 3, 5801

[16] Goban A, Choi K S, Alton D J, et al. Demonstration of a state-insensitive, compensated nanofiber trap. Phys Rev Lett, 2012, 109, 033603

[17] Zhu H, Zhao M M, Zhou J K, et al. Surface states as electron transfer pathway enhanced charge separation in TiO_2 nanotube water splitting photoanodes. Appl Catal B, 2018, 234, 100

[18] Sachs M, Pastor E, Kafizas A, et al. Evaluation of surface state mediated charge recombination in anatase and rutile TiO_2. J Phys Chem Lett, 2016, 7, 3742

[19] Zheng J W, Mo L E, Chen W C, et al. An investigation of surface states energy distribution and band edge shifts in solar cells based on TiO_2 submicrospheres and nanoparticles. Electrochimica Acta, 2017, 232, 38

[20] Sidorova T. A model of electron tunneling to the surface states in TiO_2 with application to photocatalysis. Int J Nanosci, 2019, 18, 1940034

[21] Fàbrega C, Monllor-Satoca D, Ampudia S, et al. Tuning the fermi level and the kinetics of surface states of TiO_2 nanorods by means of ammonia treatments. J Phys Chem C, 2013, 117, 20517

[22] Huber R, Spörlein S, Moser J E, et al. The role of surface states in the ultrafast photoinduced electron transfer from sensitizing dye molecules to semiconductor colloids. J Phys Chem B, 2000, 104, 8995

[23] Antuch M, Millet P, de Iwase A, et al. The role of surface states during photocurrent switching: Intensity modulated photocurrent spectroscopy analysis of $BiVO_4$ photoelectrodes. Appl Catal B, 2018, 237, 401

[24] Hossain M K, Mortuza A A, Sen S K, et al. A comparative study on the influence of pure anatase and Degussa-P25 TiO_2 nanomaterials on the structural and optical properties of dye sensitized solar cell (DSSC) photoanode. Optik, 2018, 171, 507

[25] Kim C K, Ji J M, Zhou H, et al. Tellurium-doped, mesoporous carbon nanomaterials as transparent metal-free counter electrodes for high-performance bifacial dye-sensitized solar cells. Nanomaterials, 2019, 10, E29

[26] Mehra S, Bishnoi S, Jaiswal A, et al. A review on spectral converting nanomaterials as a photoanode layer in dye-sensitized solar cells with implementation in energy storage devices. Energy Storage, 2020, 2, e120

[27] Tehare K K, Navale S T, Stadler F J, et al. Enhanced DSSCs performance of TiO_2 nanostructure by surface passivation layers. Mater Res Bull, 2018, 99, 491

[28] Gopakumar G, Ashok A, Vijayaraghavan S N, et al. MoO_3 surface passivation on TiO_2: An efficient approach to minimize loss in fill factor and maximum power of dye sensitized solar cell. Appl Surf Sci, 2018, 447, 554

[29] Roelofs K E, Brennan T P, Dominguez J C, et al. Effect of Al_2O_3 recombination barrier layers deposited by atomic layer deposition in solid-state CdS quantum dot-sensitized solar cells. J Phys Chem C, 2013, 117, 5584

[30] Pascoe A R, Bourgeois L, Duffy N W, et al. Surface state recombination and passivation in nanocrystalline TiO_2 dye-sensitized solar cells. J Phys Chem C, 2013, 117, 25118

[31] Prasittichai C, Hupp J T. Surface modification of SnO_2 photoelectrodes in dye-sensitized solar cells: Significant improvements in photovoltage via Al_2O_3 atomic layer deposition. J Phys Chem Lett, 2010, 1, 1611

[32] Palomares E, Clifford J N, Haque S A, et al. Slow charge recombination in dye-sensitised solar cells (DSSC) using Al_2O_3 coated nanoporous TiO_2 films. Chem Commun (Camb), 2002, 14, 1464

[33] Wang Y J, Bai W K, Han S L, et al. Promoted photoelectrocatalytic hydrogen production performance of TiO_2 nanowire arrays by Al_2O_3 surface passivation layer. Curr Catal, 2017, 6, 50

[34] Jeong J A, Kim H K. Thickness effect of RF sputtered TiO_2 passivating layer on the performance of dye-sensitized solar cells. Sol Energy Mater Sol Cells, 2011, 95, 344

[35] Shanmugam M, Jacobs-Gedrim R, Durcan C, et al. 2D layered insulator hexagonal boron nitride enabled surface passivation in dye sensitized solar cells. Nanoscale, 2013, 5, 11275

[36] Yang X J, Zhao L, Lv K, et al. Enhanced efficiency for dye-sensitized solar cells with ZrO_2 as a barrier layer on TiO_2 nanofibers. Appl Surf Sci, 2019, 469, 821

[37] van Delft J A, Garcia-Alonso D, Kessels W M. Atomic layer deposition for photovoltaics: Applications and prospects for solar cell manufacturing. Semicond Sci Technol, 2012, 27, 074002

[38] Vasanth A, Powar N S, Krishnan D, et al. Electrophoretic graphene oxide surface passivation on titanium dioxide for dye sensitized solar cell application. J Sci: Adv Mater Devices, 2020, 5, 316

[39] Flynn C J, McCullough S M, Oh E, et al. Site-selective passivation of defects in NiO solar photocathodes by targeted atomic deposition. ACS Appl Mater Interfaces, 2016, 8, 4754

[40] Sun H, Kurotaki H, Kanomata K, et al. ZnO/TiO_2 core-shell photoelectrodes for dye-sensitized solar cells by screen printing and room temperature ALD. Microsyst Technol, 2018, 24, 647

[41] Bakke J R, Pickrahn K L, Brennan T P, et al. Nanoengineering and interfacial engineering of photovoltaics by atomic layer deposition. Nanoscale, 2011, 3, 3482

[42] Li L P, Chen S K, Xu C, et al. Comparing electron recombination via interfacial modifications in dye-sensitized solar cells. ACS Appl Mater Interfaces, 2014, 6, 20978

[43] Fei C B, Tian J J, Wang Y J, et al. Improved charge generation and collection in dye-sensitized solar cells with modified photoanode surface. Nano Energy, 2014, 10, 353

[44] Kim S A, Abbas M A, Lee L, et al. Control of morphology and defect density in zinc oxide for improved dye-sensitized solar cells. Phys Chem Chem Phys, 2016, 18, 30475

[45] Arthi G, Archana J, Navaneethan M, et al. Hydrothermal growth of ligand-passivated high-surface-area TiO_2 nanoparticles and dye-sensitized solar cell characteristics. Scr Mater, 2013, 68, 396

[46] Rhee S W, Choi H W. Influence of RF magnetron sputtering condition on the ZnO passivating layer for dye-sensitized solar cells. Trans Electr Electron Mater, 2013, 14, 86

[47] Lee S Y, Kim S H. Deposition of TiO_2 passivation layer by plasma enhanced chemical vapor deposition between the transparent conducting oxide and mesoporous TiO_2 electrode in dye sensitized solar cells. Jpn J Appl Phys, 2012, 51, 10NE19

[48] Neo C Y, Ouyang J Y. Precise modification of the interface between titanium dioxide and electrolyte of dye-sensitized solar cells with oxides deposited by thermal evaporation of metals and subsequent oxidation. J Power Sources, 2011, 196, 10538

[49] Jin Y S, Choi H W. Properties of dye-sensitized solar cells with TiO_2 passivating layers prepared by electron-beam evaporation. J Nanosci Nanotechnol, 2012, 12, 662

[50] Tétreault N, Heiniger L P, Stefik M, et al. Atomic layer deposition for novel dye-sensitized solar cells. ECS Trans, 2019, 41, 303

[51] Zafar M, Kim B, Kim D H. Improvement in performance of inverted polymer solar cells by interface engineering of ALD ZnS on ZnO electron buffer layer. Appl Surf Sci, 2019, 481, 1442

[52] Cossuet T, Appert E, Chaix-Pluchery O, et al. Epitaxial TiO_2 shell grown by atomic layer deposition on ZnO nanowires using a double-step process and its beneficial passivation effect. J Phys Chem C, 2020, 124, 13447

[53] Kim D H, Losego M D, Peng Q, et al. Atomic layer deposition for sensitized solar cells: Recent progress and prospects. Adv Mater Interfaces, 2016, 3, 1600354

[54] Guerra-Nuñez C, Park H G, Utke I. Atomic layer deposition for surface and interface engineering in nanostructured photovoltaic devices. In: Atomic Layer Deposition in Energy Conversion Applications. Weinheim, Germany: Wiley-VCH Verlag GmbH & Co. KGaA, 2017, 119

[55] Paula L F, Hofer M, Lacerda V P B, et al. Unraveling the photocatalytic properties of TiO_2/WO_3 mixed oxides. Photochem Photobiol Sci, 2019, 18, 2469

Arya Babu received her Master degree in Nanoscience and Nanotechnology in 2020 from Amrita Centre for Nanosciences and Molecular Medicine, Kochi, India. Her major research is focusing on the development of semiconductor nanostructures for energy conversion applications.

Mariyappan Shanmugam received PhD degree from South Dakota State University, USA, in 2011. He is currently working at Amrita Centre for Nanosciences and Molecular Medicine, Kochi, India. He carried out his postdoctoral research at the College of Nanoscale Science and Engineering, State University of New York and Worcester Polytechnic Institute during 2011–2015. His major research is on the development of semiconductor nanostructures and 2D-layered materials for Optoelectronics.